Lasers in Manufacturing Conference 2019

Laserbeam-Submerged Arc Hybrid Welding – a welding technique for thick metal sheets

Uwe Reisgen[a], Simon Olschok[a], Oliver Engels[a]*

[a]*Welding and Joining Institute, RWTH Aachen University, Pontstraße 49, 52062 Aachen, Germany*

Abstract

Industrial welding of structural steel in 40 mm plate thickness range is generally carried out by using a submerged-arc welding process. Due to the high number of welding layers and the associated high energy input, thermal distortion is often unavoidable. In addition, large quantities of filler metal are required. The laserbeam-submerged arc hybrid welding process combines the conventional submerged-arc welding process with a laserbeam-welding process to form a hybrid process and thus offers great potential to replace the existing manufacturing process. With the layer/counterlayer technique, sheet thicknesses of 40 mm could already be joined flawlessly in just two welding layers. In this paper the hybrid character of the new joining process is emphasized. The mixing of the filler material down to the root area of the weld seam is proven. In addition, the welding results achieved with the hybrid welding process on material 1.4301 are presented and discussed.

Keywords: Hybrid Welding, Thick Metal Sheets, Submerged Arc Welding

1. Introduction/Motivation

Welding of structural steel with sheet thicknesses of 40 mm and more is one of the most common processes in pipe production, Houldcroft, 1989, or in the field of wind power (production of foundation- and tower-structures) Hoops et al., 2011. The joint surfaces of the joining partners are provided with a double-V-weld seam preparation, positioned to each other and are tack-welded by conventional gas metal arc (GMA)

* Corresponding author. Tel.: +49 241 80 97234; fax: +49 241 80 92170.
E-mail address: engels@isf.rwth-aachen.de

welding methods. This is followed by various welding beads with the submerged-arc (SA) welding process to fill the welding joint, Houldcroft, 1989. Depending on the sheet thickness, the volume of the weld gap to be filled increases, so that especially for large sheet thicknesses, in addition to a large quantity of welding filler material, the main welding time constitutes a significant part of the production time. In addition, thermal straightening of the produced components is usually unavoidable due to the high and asymmetrical energy input, Reisgen and Stein, 2016.

In order to replace the SA-welding process with an efficient welding process, beam welding processes such as laser beam welding (LB) and electron beam welding are used. However, practical application is often difficult due to the large component dimensions and component-tolerances. Hybrid welding processes such as the laser beam gas metal arc hybrid welding process (LAHW) can be an adequate alternative here. Sheet thicknesses of up to 20 mm and 23 mm were welded with this welding process, Vollertsen et al., 2010, Seffer et al., 2012. Pores remaining in the weld seam prove to be problematic, especially with large welding depths. The molten pool solidifies before gas bubbles rise from the deep weld regions and can escape over the surface, Seiji et al., 2006 and Kaplan et al., 2003.

Due to increasing the solidification interval, the GMAW-process was substituted by an SA-welding process. This results in a higher energy input and more time for the gas bubbles to degas through the workpiece-surface. Already in 2004 first investigations with the laser beam submerged arc hybrid welding process (SA-LAHW) using a CO_2-laser were carried out, Dilthey and Olschok, 2004 and Reisgen and Olschok, 2009. However, the process stability is described as low, Kah, 2012. In later examinations, welding of metal sheets with a thickness of 36 mm becomes possible by using a disk-laser. But also significant differences between the upper SA-dominated weldseam area and the lower LB-dominated weldseam area regarding the notch bar impact values were observed, Reisgen et al., 2012. New investigations have shown that joining plate thicknesses of up to 50 mm is possible with SA-LAHW, Reisgen et al., 2014. In addition, it was possible to significantly increase the process stability, Reisgen et al., 2016 and Reisgen et al., 2017.

In the context of this work, investigations are presented which underline the hybrid properties of the SA-LBHW process. In addition, investigations of the welding process on an austenitic chromium-nickel steel are introduced.

2. Setup

The figure below schematically shows a longitudinal section through the process zone and shows the plant structure as a CAD-model as well photographically, Fig. 1.

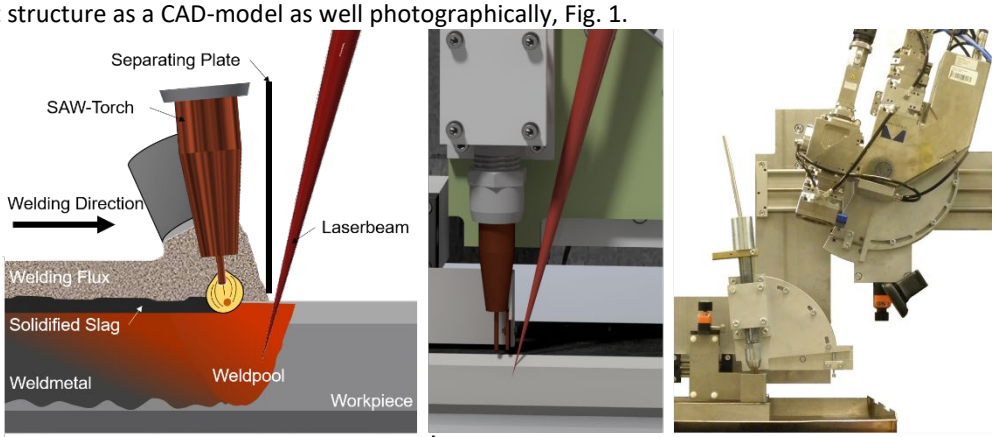

Fig. 1. (a) process zone, schematic; (b) process zone, CAD-Model; (c) hybrid welding head

The leading laser beam and the trailing submerged arc torch can be detected. A separating plate is positioned between the two components with the aim of separating the welding powder required for the submerged arc welding process from the effective area of the laser beam. The angles of incidence of the submerged arc torch and the LBW optics in relation to the workpiece perpendiculars are of decisive relevance for the welding result. The process distance (distance from the center of the wire electrode to the point of impact of the laser beam relative to the workpiece surface) is also an important setting parameter.

For the welding results presented below, a mild steel (S355) and an austenitic chromium-nickel steel (1.4301) with a sheet thickness of 40 mm were used. The metallurgical compositions are listed in Table 1 (weight percent; balance: iron).

Table 1. chemical composition base metal

Base metal	C	Si	Mn	P	Cr	Ni	Cu
	[%]	[%]	[%]	[%]	[%]	[%]	[%]
S355	0.033	0.33	1.52	0.009	0.15	0.013	0.017
1.4301	0.02	0.31	1.07	0.032	18.82	7.88	0.299

Two different welding wire/flux combinations were used as welding filler materials. The welding powder used for the mild steel has the standard designation SA FB 1 55 AC H5 and a basicity of 3.2. The welding powder used for the stainless steel has the standard designation SA FB 2 55 53 AC and a nominal basicity of 2.5. The welding wire electrodes each have a diameter of 4 mm. The chemical composition is shown in Table 2 (weight percent; balance: iron).

Table 2. chemical compositon wire electrode

Wire electrode	C	Si	Mn	Ni	Cr
	[%]	[%]	[%]	[%]	[%]
T3Ni1 (for S355)	0.07	0.3	1.7	0.8	/
S19 9 L (for 1.4301)	0.02	0.4	1.9	9.8	19.8

3. Welding trials

3.1 Hybrid character

In the work mentioned in the introduction, it was found that the process distance has a decisive influence on whether a serial or purely hybrid welding process occurs. It could be shown that a process distance of 15 mm at a laser beam power of 16 kW, a travel speed of 0.6 m/min, a wire feed speed of 2.1 m/min and an angle of incidence of the laser beam of 15° leads to the formation of a hybrid welding process, Reisgen et al., 2018. To substantiate this statement, EDX analyses of the depth of the weld seam were prepared and evaluated with regard to the nickel contained only in the filler material. The difference between a serial SA-LAHW weld and a hybrid weld is shown in Figure 2. The serial weld, Figure 2 (a), has a nickel content of about 0.7 % in the SA-dominated region, while the LB-dominated region has only about 0.2 %. The transition between these two areas occurs abruptly. This indicates that there are two separated weld seam areas. The hybrid weld, Figure 2 (b), has a uniform decreasing nickel content. This indicates that there is a common weld pool.

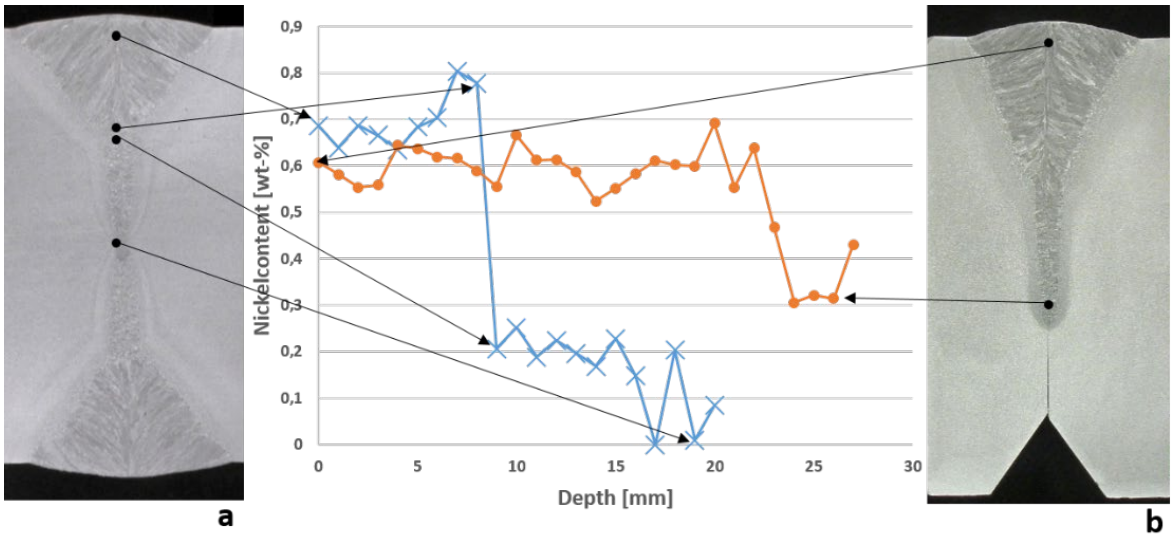

Fig. 2. EDX-analysis along the depth of the weld seam (wt. %); (a) D_{LA}= 24mm; (b) D_{LA}= 15mm; Reisgen et al., 2018

Furthermore, the weld samples welded with a laserpower of 16 kW, travel speed of 0.6 m/min, wire feed speed of 2.1 m/min and angle of incidence of the laser optics of 15° were subjected to notch bar impact tests. It is expected that the areas "SA-dominated", "Transition area" and "LB-dominated" of a hybrid weld have comparable values at the same testing temperature. So in another way, the homogeneity of a hybrid SA-LAHW weld seam is shown. Table 3 summarizes the average results of the notched-bar testings.

Table 3. Average notched-bar impact energies; N1 - SA FB 1 55 AC H5

Testing temperature [°C]	Impact-energy (LB-dominated) [J]	Impact-energy (SA-dominated) [J]	Impact-energy (Transition area) [J]
20	300	231,6	290
0	300	212,2	273
-20	201,5	195,2	271,8
-40	82,00	153,2	185,8
-60	107,5	133,4	91,8
-80	72	72,8	88

Fig. 3 summarizes the results of the notched-bar testings in a diagram.

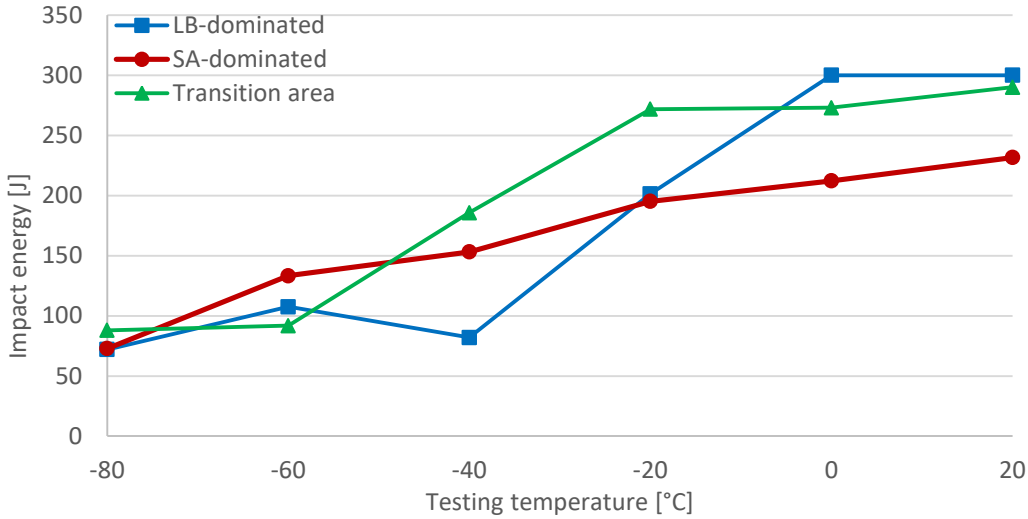

Fig. 3. notched impact energy - Diagram; Ni1 - SA FB 1 55 AC H5

The SA-dominated weld seam has a uniformly decreasing course with decreasing test temperatures. At room temperature a notched bar impact energy of 230 J is achieved. At -20°C the notched bar impact energy is 195 J. At a test temperature of -60°C a notched bar impact energy of 133 J was determined. The transition area also has a uniformly decreasing course of the notched bar impact energy with decreasing test temperature. At room temperature a notched bar impact energy of 290 J is achieved. At -20°C about 270 J are achieved. At a test temperature of -60°C, an impact energy of 90 J could be determined. The LB-dominated weld seam area has a notched bar impact energy of more than 300 J at room temperature and 0°C. At a test temperature of -20°C, the notched bar impact energy drops to about 200 J. For -40°C and lower test temperatures, notched bar impact energy between 80 J and 105 J is determined.

Above all, it should be emphasized that the notched bar impact values determined from the three weld seam areas show comparable values at the respective test temperature. This is further evidence that the filler material has been mixed up down to the deep weld seam areas. The strongly differing results of the LB- and SA-dominated areas as shown in, Reisgen et al., 2012, cannot be observed.

3.2 Stainless steel

Furthermore, the transferability of the welding results achieved on mild steel to a stainless steel was tested. In particular, the material 1.4301 with a sheet thickness of 40 mm was welded with the welding electrode/flux combination S19 9 L + SA FB 2 55 53 AC which is suitable for this material. The chemical compositions are given in Table 1 and Table 2. The weld seam preparation and the tacking concept of the two joining partners remain unchanged.

The first welding test was carried out with a laser beam power of 16 kW, a feed speed of 1.2 m/min, a process distance of 15 mm and activated laser beam oscillation (amplitude 1.5 mm; frequency 100 Hz). The wire feed speed is 2.1 m/min (leads to an adequate filling degree). The corresponding macrosection is shown in Fig. 4.

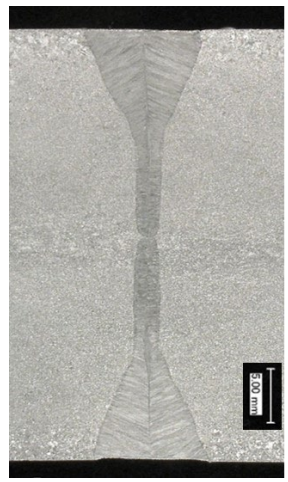

Fig. 4. Crosssection; 1.4301; P_L= 16 kW, v_S= 1,2 m/min, A= 1,5 mm

Welding defects in the form of pores or linear defects cannot be detected. The welding depth is 20 mm. A uniform transition of the growth direction of the dendrites from the SA-dominated to the LB-dominated weld area can be detected. When looking at the outer seam pattern, it is noticeable that the width of the upper bead varies greatly. Also during the welding it could be observed that the welding process is subject to irregularities. Since the weld metal has a greater fluidity than the weld metal of the mild steel, molten metal is often pushed into the effective range of the laser beam.

Fig. 5 shows the result of two different welds. Both weld samples were welded with a laser beam power of 16 kW, a feed rate of 0.8 m/min and a process distance of 15 mm. Fig. 5 (top) was welded with laser beam oscillation switched on (amplitude 1.5 mm; frequency 100 Hz) and Fig. 5 (bottom) without laser beam oscillation.

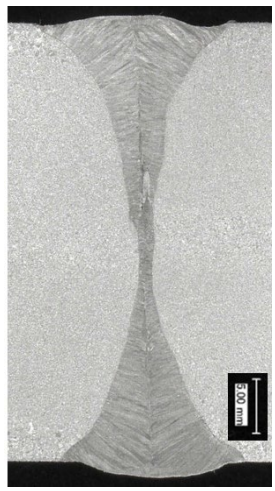

Fig. 5. Crosssection; 1.4301; P_L= 16 kW, v_S= 0.8 m/min, A= 1.5 mm (top); P_L= 16 kW, v_S= 0.8 m/min, A= 0 (bottom)

No weld defects in the form of pores or linear defects can be detected in either weld seam. The welding depth for the weld seam with laser beam oscillation (top) is approximately 21 mm. The welding depth for the weld seam without laser beam oscillation (bottom) is about 25 mm. As expected, the LB-dominated area of the upper weld seam is wider than that of the lower weld seam. Both weld seams show a conspicuously uniform geometric transition from the SA- to the LB-dominated weld seam area. The growth direction of the dendrites also changes extremely uniformly. The outer seam pattern again shows fluctuations in width for both welds. Analyses of the chemical composition of the weld metal have shown that the alloying elements are homogeneously distributed over the entire depth of the weld seam. A complete mixing within the molten pool has therefore taken place.

Fig. 6 shows two different welds. Fig. 6 (top) shows the cross section of a weld seam which is welded with a laser beam power of 14 kW, a feed rate of 0.6 m/min and a process distance of 15 mm. Fig. 6 (bottom) was welded with a laser beam power of 16 kW, a feed rate of 1 m/min and a process distance of 15 mm. Both welds were performed without laser beam oscillation.

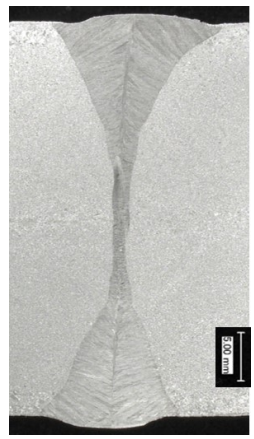

Fig. 6. Crossection; 1.4301 P_L= 14 kW, v_S= 0.6 m/min, A= 0 (top); P_L= 16 kW, v_S= 1m/min, A= 0 (bottom)

No weld defects in the form of pores or linear defects can be detected in either weld seam. The upper weld seam with a laser beam power of 14 kW reaches a welding depth of about 22 mm. The lower weld seam with a laser beam power of 16 kW reaches a welding depth of about 25 mm. Both welds have a uniform geometric transition from the SA- to the LB-dominated weld area.

Fig shows microscopic images of a weld sample which was welded with a feed rate of 0.8 m/min, a laser beam power of 16 kW and activated laser beam oscillation (amplitude 1.5 mm; frequency 100 Hz). Shown is the weld metal, Fig (top left), the fusion line, Fig (bottom left), and the root area, Fig (right). No defects are visible in the microsections shown.

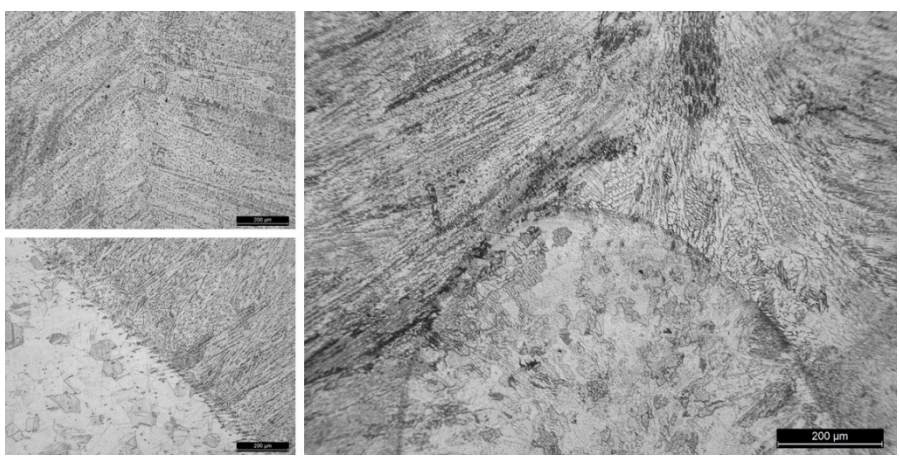

Fig. 7. Microsection; 1.4301; weld metal (top left); fusion line (bottom left); root area (right)

In addition, notched bar impact bending tests were also carried out for this base material. Table 4 summarizes the average results of the notched bar impact tests.

Table 4. Average notched impact energy; S19 9 L + SA FB 2 55 53 AC

Testing temperature [°C]	Impact-energy (LB-dominated) [J]	Impact-energy (SA-dominated) [J]
20	113,5	146
0	139,2	140
-20	142	114,67
-40	93,00	122,40
-60	102	109,6
-80	100	102

Fig. 8. summarizes the results of the notched bar impact tests in a diagram.

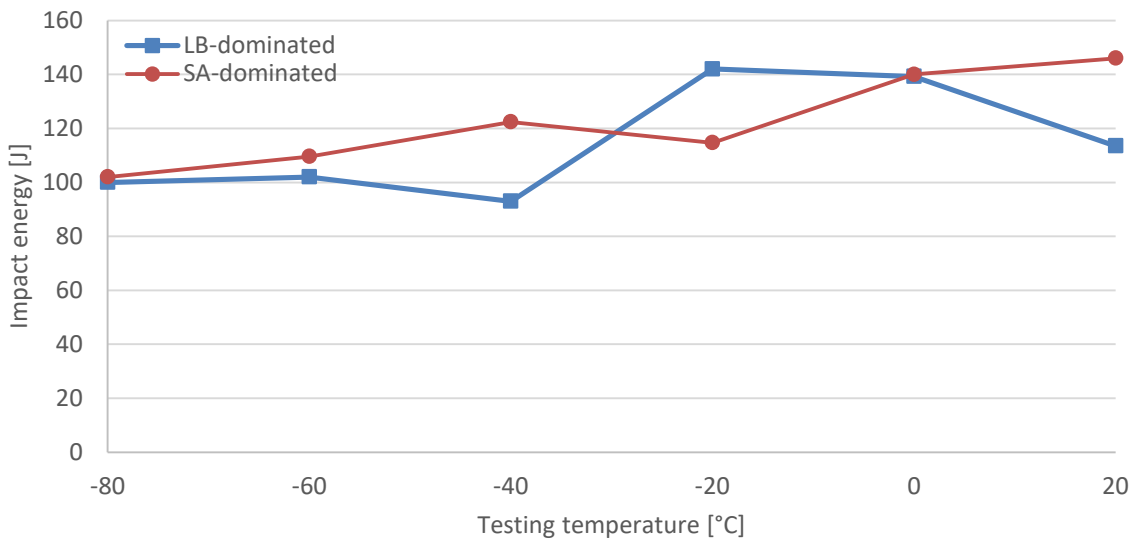

Fig. 8. Notched impact energy diagram; S19 9 L + SA FB 2 55 53 AC

The SA-dominated weld area shows a uniform drop in impact energy at decreasing test temperatures. Whereas an impact energy of 145 J could be determined at room temperature, the impact energy already drops to 115 J at a test temperature of -20°C. The impact energy of the weld seam is uniform at decreasing test temperatures. For a temperature of -60°C about 100 J could be reached. The LB-dominated weld seam area has a notched bar impact energy 110 J at room temperature. At a test temperature of -20°C, 140 J can be achieved. At -60°C the average notched bar impact energy is about 100 J.

The fact that the two curves show such comparable values for the notched bar impact energy also shows here that a mixing of the molten pool has taken place and a weld seam with homogeneous properties has been produced.

4. Conclusion/Outlook

In this thesis, the different areas of weld specimens produced with the SA-LAHW-process were subjected to notched bar impact tests. The results were compared in a diagram. It can be seen that the results for the different weldseam areas achieved in the notched bar impact tests are very close to each other. Thus, homogeneous weld seam properties with regard to the notched bar impact strength are prensent over the entire weld seam depth.

Furthermore, high quality welds were produced on material 1.4301. An optically good mixing of the weld seam area could be achieved. Notched bar impact bending tests were also carried out. Here, too, it could be demonstrated that homogeneous notched bar impact toughness are present over the depth of the weld seam.

In subsequent work, the focus of the investigations will be on gap bridgeability with the SA-LAHW. Joint gap widths of up to 3 mm are to be tested in detail. Furthermore, the classical GMA-LAHW-process shall be compared with the SA-LAHW-process and investigated with regard to the melt pool mixing.

Acknowledgements

The IGF project "Testing of the laser beam submerged-arc hybrid welding process for industrial applications in the field of large plate thicknesses (LUPuS)", IGF project no. 19.039 N, of the Research Association for Steel Applications. FOSTA, Sohnstraße 65, 40237 Düsseldorf, was funded by the AiF within the framework of the programme for the promotion of industrial joint research (IGF) of the Federal Ministry of Economics and Energy on the basis of a decree of the German Bundestag.

Gefördert durch:

Bundesministerium
für Wirtschaft
und Energie

aufgrund eines Beschlusses
des Deutschen Bundestages

References

Houldcroft, P.T., 1989. Submerged-Arc Welding, Woodhead Publishing Series in Welding and other Joining Technologies, Woodhead Publishing , p. 9 – 26

Hoops, K., Schumacher, P., 2011. Wirtschaftliche schweißtechnische Produktion von Großkomponenten für Offshore-Windenergieanlagen, DVS-Berichte Band 277, Schweißen im Schiffbau und Ingenieurbau, p. 47 – 52

Reisgen, U., Stein, L.,2016, Fundamentals of Joining Technologies – Welding, Brazing and Adhesive Bonding, DVS-Media, Duesseldorf, p. 119 – 132

Vollertsen, F., Rethmeier, M., Gumenyuk, A., Gruenewald, S., Reisgen, U., Olschok, S., 2010, Welding thick steel plates with fibre lasers and GMAW, Welding in the World 54, p. 62 -70

Seffer, O., Lindner, J., Springer, A., Kaierle, S., Wesling, V., Haferkamp, H., 2012, Laser GMA hybrid welding for thick wall applications of pipeline steel with grade X70, International Congress of Applications of Lasers and Electro Optics, Anaheim, Laser Institute of America, Orlando, p. 494 - 501

Seiji, K., Yasuaki, N., Satoru, U., Masami, M., 2006, Physical phenomena porosity mechanism in laser-arc hybrid welding, Trans. JWRI 35, p. 13 – 18

Kaplan, A., Mizutani, M., Katayama, S., Matsunawa, A., 2003, First international Symposium on high-power laser macroprocessing, Proc. SPIE 4831, p. 1 - 6

Dilthey, U., Olschok, S., 2004, Abschlussbericht des AiF-Forschungsvorhabens 13.407 N

Reisgen, U., Olschok, S., 2009, Laser-submerged arc hybrid welding, Paton Welding Journal 4, p. 38

Kah, P., 2012, Overview of the exploration status of laser-arc hybrid welding processes, Rev. Adv. Mater. Sci. 30, p. 120 – 121

Reisgen, U., Olschok, S., Jakobs, S., Schleser, M., Mokrov, O., Rossiter, E., 2012, Laser beam submerged arc hybrid welding, Physics Procedia 39, p. 75 - 83

Reisgen, U., Olschok, S., Jakobs, S., 2014, Laser submerged arc hybrid welding (LUPuS) with solid state lasers, Physics Procedia 56, p. 653 – 662

Reisgen, U., Olschok, S., Jakobs, S., Engels, O., 2016, Modern hybrid welding process for structural steelwork engineering – Laser submerged arc hybrid welding, Journal of Laser Applications 28, 022011

Reisgen, U., Olschok, S., Engels, O., 2017, Innovative hybrid welding process for structural steelwork engineering – Laser submerged arc hybrid welding, Journal of Laser Applications 29, 022041